ISSN 0036-0244, Russian Journal of Physical Chemistry A, 2019, Vol. 93, No. 10, pp. 1984–1993. © Pleiades Publishing, Ltd., 2019.
Russian Text © The Author(s), 2019, published in Zhurnal Fizicheskoi Khimii, 2019, Vol. 93, No. 10, pp. 1575–1583.

ON THE 90th ANNIVERSARY OF THE DEPARTMENT OF CHEMISTRY OF THE MOSCOW STATE UNIVERSITY

NiMo and NiW Nanostructured Catalysts of Thiophene Oxidation, Obtained via Laser Electrodispersion

A. A. Bryzhin[a,*], I. G. Tarkhanova[a], K. I. Maslakov[a], S. A. Nikolaev[a], S. A. Gurevich[b], V. M. Kozhevin[b], D. A. Yavsin[b], M. G. Gantman[c], and T. N. Rostovshchikova[a]

[a] *Faculty of Chemistry, Moscow State University, Moscow, 119991 Russia*
[b] *Ioffe Institute of Physics and Technology, Russian Academy of Sciences, St. Petersburg, 194021 Russia*
[c] *Friedrich-Alexander-Universität Erlangen–Nürnberg, 91054 Erlangen, Germany*
**e-mail: itar_msu@mail.com*

Received March 15, 2019; revised March 15, 2019; accepted April 9, 2019

Abstract—New bimetallic catalysts based on Ni and Mo or W oxide nanoparticles deposited on alumina are obtained via the laser electrodispersion of tightly compacted binary mixtures of NiMo and NiW powders. SEM, TEM, and XPS show that both components of each pair are uniformly distributed over a carrier's surface in the form of nanoparticles of 4–7 nm in size. Metals on the catalyst's surface are predominantly in an oxidized state. The catalytic activity of $NiMo/Al_2O_3$ and NiW/Al_2O_3 pairs is compared using examples of the oxidation of thiophene and dibenzothiophene by hydrogen peroxide. High reagent conversion on such catalysts with ultra-low metal contents (<0.01 wt %) is maintained by continually repeating the process. Introducing a sulfated zwitterionic liquid into the reaction mixture results in additional improvement of catalyst efficiency.

Keywords: nanoparticles, laser electrodispersion, catalysis, oxidation, thiophene
DOI: 10.1134/S0036024419100029

INTRODUCTION

Traditional chemical ways of synthesizing bimetallic catalysts have a number of considerable drawbacks associated with the uneven filling of a carrier's surface with active components, wide distributions of particle sizes, and insufficient reproducibility of their properties, due to the strong effect the conditions of preparation have on the structure of the resulting materials. In addition, they are multistep processes that in most cases require the use of precursors, stabilizers, and other chemical reagents that affect the environment.

Means of physical synthesis based most often on laser ablation [1, 2] normally ensure a more uniform distribution of active components over a catalyst's surface, have only one step, and are more environmentally friendly. Plasma electrolytic oxidation (PEO) also allows us to form in one step oxide coatings of a given composition that display catalytic activity in oxidative processes and enhanced chemical and thermal stability [3]. However, this technique requires the use of electrolyte solutions and assumes a high content of active components in the catalyst's composition. Without the use of chemical precursors, reducing agents, or stabilizers, laser electrodispersion (LED) allows us to obtain so-called "crusty" catalysts, in which mono- and bimetallic particles of a strictly fixed size are uniformly distributed over the external surface of the carrier [4–6]. In terms of adsorption and catalytic properties, low-percentage LED catalysts differ from similar materials obtained by such traditional means as impregnation, ion exchange, metal–vapor synthesis, and precipitation from colloidal dispersions [7, 8]. Catalysts based on nickel nanoparticles deposited on Al_2O_3 via LED are especially active in the oxidation of CO with an extremely low Ni content of 0.01 wt %, while Ni/Al_2O_3 catalyst obtained via impregnation is virtually inactive [9]. This difference is most likely due to nickel being present in the LED coatings in two electronic states, Ni^0 and Ni^{2+}, which is not observed in traditional catalysts containing only NiO. According to data from scanning tunneling microscopy/scanning tunneling spectroscopy (STM/STS) [10], nanoparticles formed via LED are amorphous, heterogeneous in composition, and include regions with metallic and zero conductivity that correspond to nickel oxides of probably nonstoichiometric composition. This could be the reason for their increased activity in oxidation.

In this work, LED was used for the first time to form bimetallic coatings based on Ni and Mo or W on surfaces of aluminum oxide, using tightly pressed two-component mixtures of powders as targets. In [4, 5], bimetallic coatings were produced via LED through the successive deposition of two components, or from

Table 1. Catalyst characteristics

nos.	Catalyst/Carrier	*r*, mm	τ, min	*m*, mg	$C \times 10^3$, wt %	Calculated [Ni]/[M] atomic percentage ratio
1	Ni/Mo/AI-05	1.6–1.8	12.0	0.077	3.9	0.71
2	Ni/W/AI-05	1.6–1.8	24.0	0.146	7.3	1.33
3	Ni/W/AOK-63-11	0.4–1.0	18.0	0.11	5.5	1.33

r is the size of granules, τ is the length of deposition, *m* is the mass of the deposited mixture, and *C* is the total metal content.

a prefabricated metal alloy. The aim of this work was to identify the structural features and catalytic behavior of new materials in the peroxidation of sulfur-containing aromatic compounds and the oxidative desulfurization of hydrocarbons. This choice was due to the relevance of desulfurization in modern petrochemistry, a result of stricter environmental requirements for different types of fuel and an increase in the share of production of sulfur and high-sulfur oil and gas. The main way of removing sulfur from petroleum products is hydrotreatment, but it does not always allow complete removal of the substituted aromatic organic sulfur compounds. Co(Ni)/Mo(W) bimetallic systems on alumina are in this case used as catalysts [11, 12]. It should be noted that this is a flammable and explosive process and is therefore done only at large processing plants, where expensive equipment can be used that fully ensures production safety. Oxidative means can be used as an alternative, as can the adsorption and extraction of organic sulfur compounds with their subsequent processing. These techniques are often used in combination, ensuring deep desulfurization. Oxide and carbon materials promoted by transition metals (Cu, Ni, Ag, and Zn) serve as solid adsorbents [13]. Catalysts of heterogeneous oxidation are of different compositions, especially individual and mixed oxides and salts containing transition metal ions in high states of oxidation (e.g., derivatives of Mo, W, V, Cr, Nb, and Ce) and binary systems (e.g., $NiO–MoO_3$, $CoO–MoO_3$) on oxide substrates [14–21]. Analysis of such compositions shows that many of them simultaneously exhibit properties of both catalysts and adsorbents. In addition, Ni-containing compositions can serve as adsorbents and catalysts in two processes: hydrogenation and oxidation [11, 12, 22, 23]. Such polyfunctional catalysts are of particular interest, since they can be used in both hydrotreatment and oxidative desulfurization [23]. In this work, bimetallic catalysts based on Ni and Mo or W on surfaces of aluminum oxide were used for the peroxide oxidation of thiophene and dibenzothiophene—typical representatives of the sulfur-containing organic compounds in hydrocarbons. When conducting a liquid-phase reaction in a hydrocarbon medium, 4-(3'-ethylimidazolium)butane sulfonate, i.e., a zwitterionic compound belonging to the class of ionic liquids (IL), was used as a stabilizer of metallic coating. In [24], we successfully used such an approach in a similar reaction with the participation of catalysts obtained via plasma electrolytic oxidation.

EXPERIMENTAL

Two types of γ-Al_2O_3 that differ in granule size were used in this work: AI-05 (specific surface area, 194 m^2/g; pore volume of 0.75 cm^3/g; granule size, 1.6–1.8 mm) and AOK-63-11 of grade B (specific surface, 180 m^2/g; pore volume, 0.55 cm^3/g; granule size, 0.4–1.0 mm). Bimetallic catalysts $NiMo/Al_2O_3$ and NiW/Al_2O_3 were obtained by depositing nanoparticles onto Al_2O_3 granules via LED in a special cell, as described in [5]. Two grams of the carrier were placed in the cell. Mixtures of Ni/Mo and Ni/W powders with a weight percentage ratio of 30/70 were prepared by cold pressing and used as targets. The grain size of Ni, Mo, and W powders manufactured by ABCR Dr. Braunagel GmbH was 3–8 μm. The content of metals in the catalyst was determined from the calibration dependences of the deposited films' rate of growth, obtained earlier using a Sycon Instruments SCT-2000A quartz thickness gauge.

The characteristics of the prepared catalysts are given in Table 1. Sample **3-IL** was obtained by keeping several granules of sample **3** and 4-(3'-ethylimidazolium)butane sulfonate (weight ratio 1 : 1) in an aqueous solution with subsequent drying at room temperature.

Compound 4-(3'-ethylimidazolium)butane sulfonate was obtained according to the standard procedure described in [25].

Microphotographs of the samples were obtained via scanning and transmission electron microscopy (SEM and TEM) on JEOL JSM 6000 NeoScope and JEOL JEM 2100F/UHR instruments with a resolution of 0.1 nm, respectively. Prior to our TEM studies, several granules of the sample were placed in alcohol and exposed to ultrasound for 300 s, as in [5]. A drop of the resulting suspension with the sample was placed on a TEM copper grid, dried for 1 hour, and investigated. The size of the deposited phases was estimated

as the maximum linear size. A qualitative analysis of the surface was performed *in situ* by means of energy dispersive analysis (EDA) using a JED-2300 instrument.

The textural characteristics of the samples before and after catalysis were determined via BET, BJH, and DFT on an Autosorb 1 instrument from Quantachrome (United States) after preliminary evacuation over 3 h at 300°C. The specific surface area and total pore volume were calculated from isotherms of nitrogen adsorption and desorption at 77 K using software included in the instrument package.

X-ray photoelectron spectra of the catalyst were recorded on an Axis Ultra DLD spectrometer (Kratos) equipped with a monochromatic AlK_a radiation source with a neutralizer. The spectra were recorded at an analyzer transmission energy of 160 eV (survey spectrum) and 40 eV (high-resolution spectra). Calibration was performed using the C1*s* component at 285.0 eV.

To perform our catalytic tests, 10 mL of the model mixture (a 1 wt % solution of thiophene or dibenzothiophene in isooctane), 0.1 g of the catalyst, and an oxidant (0.4 mL of a 50% aqueous solution of hydrogen peroxide) were placed in a thermostatted reactor. The contents of the reactor were stirred with heating (60°C), and liquid phase samples were taken periodically for analysis. A quantitative analysis of the organic phase in the reaction mixture was performed via gas–liquid chromatography on a Kristall 4000 instrument equipped with a Zebron ZB-1 capillary column (l = 30 m), filled with a liquid phase of 100% dimethyl polysiloxane, and a flame ionization detector (FID). The contents of thiophene and dibenzothiophene were determined in the linear programming mode at temperatures of 90–220°C using an internal standard. It was found that oxidation of the initial reagents (thiophene and dibenzothiophene) produced sulfuric acid and sulfone, respectively [24]. After standard 4-h tests, the liquid phase was drained, a new batch of reagents was placed in the reactor, and identical new tests were performed for five cycles. In separate experiments, fractional additions of a H_2O_2 solution in two portions of 0.2 mL each were used at intervals of 2 h. To determine the effect a zwitterionic liquid has on the efficiency of the process, 0.1 g of 4-(3'-ethylimidazolium)butane sulfonate was added to the reaction mixture.

Initial rate r_o (mol/h) of thiophene oxidation was calculated from the drop in its concentration during the first hour of the reaction. The turnover frequency (TOF) was determined by normalizing the loss of thiophene in moles during the first hour of the reaction (Δn (thiophene)/h) to the number of moles of Mo or W (n (W or Mo)) in the samples, assuming all atoms participated in the catalytic process. The calculations considered the contribution from the carrier to thiophene conversion, which was determined in independent experiments.

Twenty milliliters of diesel fuel, 0.8 mL of a 50% solution of H_2O_2, and 0.04 g of catalyst were used in testing samples during the purification of diesel fuel with a total sulfur content of 1080 ppm. The reaction was conducted for 4 h at 60°C using single or fractional additions of hydrogen peroxide with and without 0.1 g of 4-(3'-ethylimidazolium)butane sulfonate. The reaction solution was then washed twice with dimethylformamide to remove products of oxidation and analyzed on an ASE-2 X-ray fluorescence spectrometer.

RESULTS AND DISCUSSION

Catalyst Structure

The textural characteristics of the catalysts after deposition of the active components varied very slightly. For sample **3**, calculations of the average values of specific surface and total pore volume according to BET, BJH, and DFT gave values of 178 m^2/g and 0.53 cm^3/g. These were almost identical to the characteristics of the initial carrier. Similar values were obtained for other samples. In LED, the textural characteristics of the initial carriers are typically retained when synthesizing catalysts, since nanoparticles are deposited only on the external surface of the carrier without affecting the pore space [6].

However, adding an ionic liquid greatly reduces the specific surface area of a sample. For sample **3-IL**, the average values of the specific surface area and total pore volume according to the BET, BJH, and DFT data fell to 74 m^2/g and 0.28 cm^3/g. Only larger pores with diameters of around 10 nm were preserved in the modified ionic liquid sample, while small pores with diameters of 5 nm disappeared.

Typical micrographs of the surface of sample **2** are shown in Fig. 1a. The EDA spectrum of the grey surface regions (not shown) includes the Al, O, C, and Cu lines associated with aluminum oxide and the material of the grid. The EDA spectra (Fig. 1b) of the black particles contain the NiK_α (7.5 keV) and WM_α (1.8 keV) lines, allowing us to attribute them to the sites of Ni and W localization.

As can be seen from Fig. 1a, these particles were close to spherical in shape and had sizes of 4 to 7 nm. Clusters of such particles with sizes of are 50 nm are observed in some regions of the surface (Fig. 1c). As can be seen from this figure, components Ni and W were evenly distributed. The sites of Ni and W localization coincided fully in all other analyzed surface regions of the samples. For example, quantitative data on the composition of a number of selected surface regions are given in Table 2.

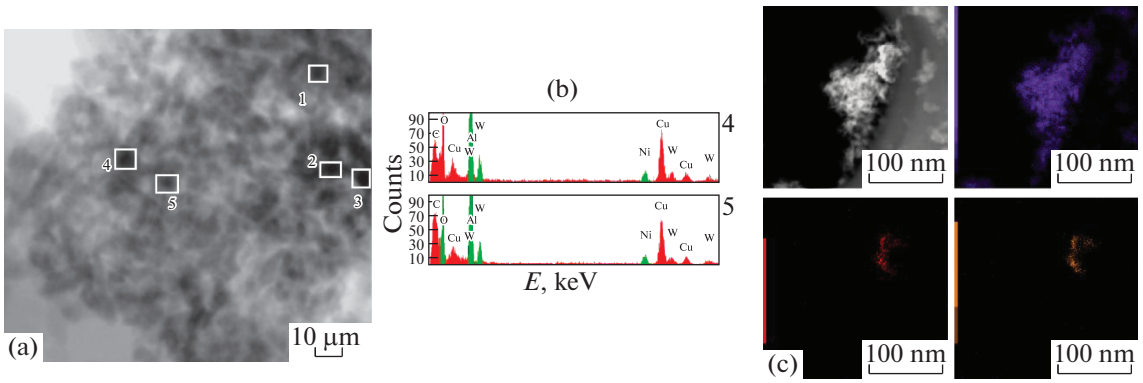

Fig. 1. (a) TEM/EDA images of the sites of Ni and W phase localization, according to our EDA data (squares); (b) examples of the integral EDA spectra for the selected points; (c) surface mapping of sample **2**.

These data show the average Ni/W atomic percentage ratio of 1.35 that was obtained experimentally was close to their ratio (1.32) in the composition of the initial target.

As can be seen from the data presented in Fig. 2, the sites of Ni and Mo localization on the surface of sample **1** also coincided. Due to its lower metal content, however, we were unable to quantify their ratio in the catalyst from the EDA data.

Figure 3 shows the SEM images and EDA results for sample **2**. These studies required no prior dispersion of samples. As is seen from our results, both metals were uniformly distributed over the surface of aluminum oxide. Their weight ratio was 34/66 (atomic ratio, 1.61), fairly close to the composition of the initial target.

Using a mixture of powders as targets for the preparation of bimetallic catalysts via LED allowed us to obtain coatings with a given ratio and uniform distribution of the active components over the surface of the carrier, as in the formation of nanoparticles from an alloy of metals [5].

Table 2. Distribution of elements over the surface of sample **2**, according to EDA

Point*	O, at %	Al, at %	Ni, at %	W, at %
1	46.2	36.1	10.4	7.3
2	35.7	36.2	16.8	11.2
3	57.4	32.6	5.4	4.6
4	56.3	38.5	2.3	2.9
5	53.0	42.9	2.0	2.1
6	49.5	40.5	6.1	3.9
	Average at %		7.2	5.3
Average Ni/W atomic percentage ratio				1.35

* Points are marked in Fig. 1a.

Since a high density of active particles was created on the external surface of the carrier by features of LED, such samples can be analyzed via X-ray photoelectron spectroscopy (XPS), but only using intact catalyst granules with no preliminary grinding.

The high resolution spectra of the Al2*p* lines were the same for all samples. They are shown in Fig. 4a for sample **1,** along with the spectra of the Ni2*p* lines (Fig. 4b). A similar spectrum of Ni was obtained for sample **2**, which was based on nickel and tungsten deposited on coarse alumina.

The bonding energy of the Al2*p* line (74.7–74.9 eV) observed in all of the spectra was somewhat higher than the typical values for aluminum oxide (74.4–74.6 eV), as was the 74.3 eV found for monometallic Ni/Al_2O_3 catalysts obtained via LED [8]. This could indicate some aluminum was included in the composition of complex oxides, most likely with molybdenum or tungsten. Figure 5 shows high-resolution XPS spectra of the Mo and W lines in samples **1** and **2**.

The spectra of the lines of nickel, molybdenum, and tungsten were decomposed into components corresponding to different states of these elements in the sample. The results are presented in Figs. 4 and 5 and given in Tables 3 and 4. In the Ni2*p*, Mo3*d*, and W4*f* XPS spectra (Figs. 4 and 5 and Tables 3 and 4), we mainly observe the contribution from the most oxidized forms of these elements (Ni^{+2}, Mo^{+6}, and W^{+6}). In addition, the Ni^0, Mo^0, and W^0 metallic states were preserved in part; the observed bonding energies of the corresponding components were close to those in metallic nickel (852.7 eV), molybdenum (228.0 eV), and tungsten (31.4 eV) [26]. Two things about the $Ni2p_{3/2}$ spectrum should be noted. First, the content of the metal component with a bonding energy of 852.8 eV was unusually high, reaching 20 and 30% in samples 1 and 2 containing molybdenum and tung-

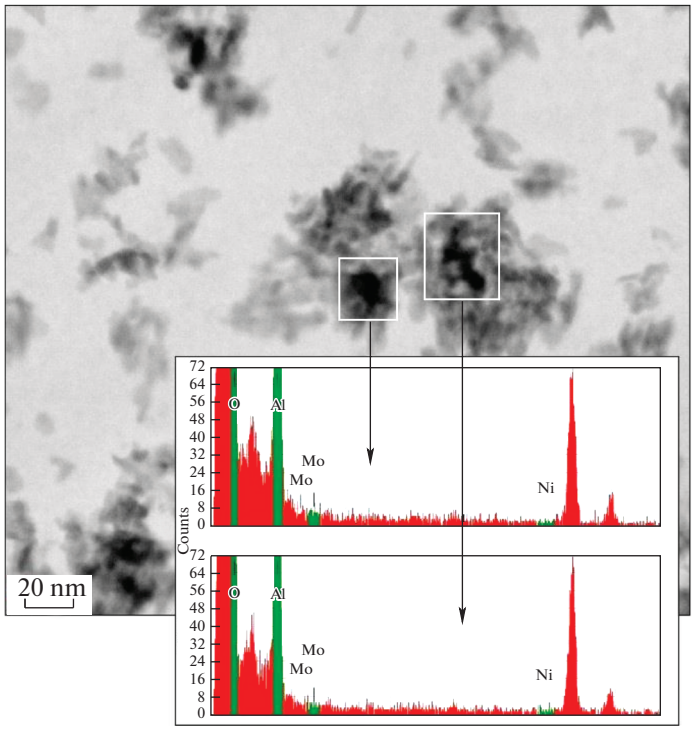

Fig. 2. TEM microphotomicrograph of sample **1**. The integral EDA spectrum from the selected locations is shown in the insert.

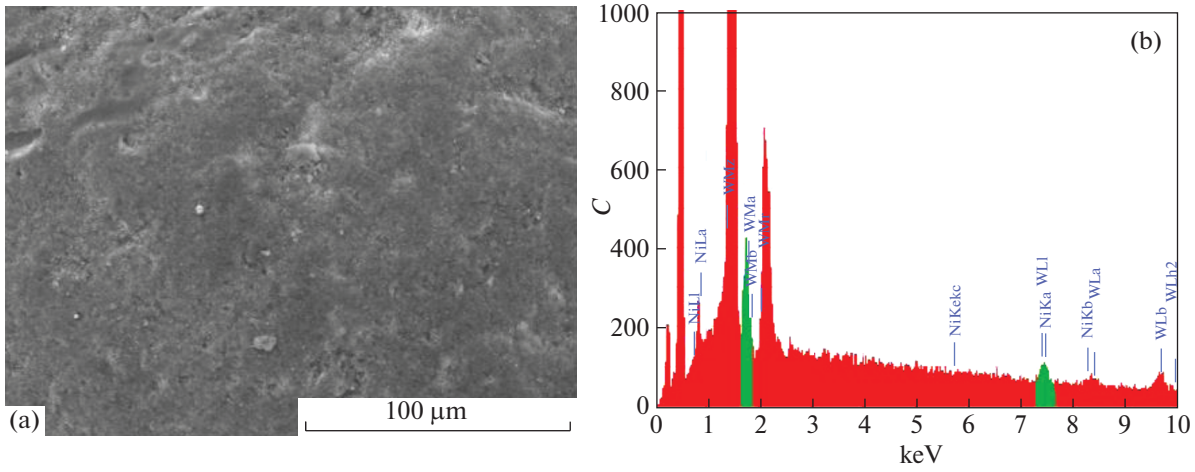

Fig. 3. SEM images and the integral EDA spectrum of sample **2**.

sten, respectively. Earlier, in analyzing monometallic Ni/Al_2O_3 samples also prepared via LED, such large amounts of Ni^0 were detected only in multilayer coatings with a high nickel content of 0.03 wt % [8, 9]. In addition, the observed spectrum of the oxidized form of Ni^{+2} differed substantially from that of NiO with a bonding energy of 854.4 eV, as was the case with the monometallic sample. This is typical of nickel hydroxide or complex oxides that contain nickel [27].

In addition to their metallic and maximally oxidized states, intermediate oxidized states of the molybdenum and tungsten in samples **1** and **2** are observed in their XPS spectra. Components with complex shapes, the presence of which was due mainly to tetravalent states of the Mo^{+4} and W^{+4}, were needed to obtain a complete description of the Mo3*d* and W4$f_{7/2}$ spectra. A similar spectrum with a complex form and a bonding energy of 229.3 eV for the Mo3$d_{5/2}$ component was attributed to oxide MoO_2 [28]. At the same

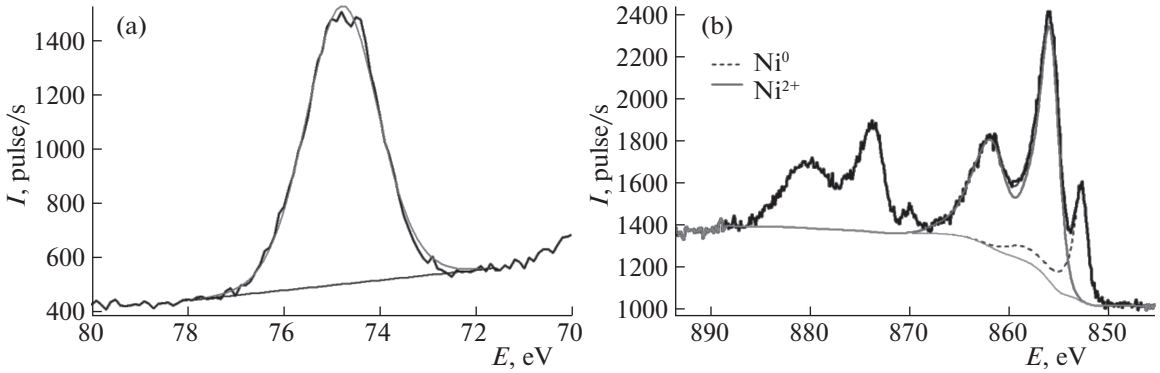

Fig. 4. (a) Al2*p* and (b) Ni2*p* XPS spectra of sample **1**.

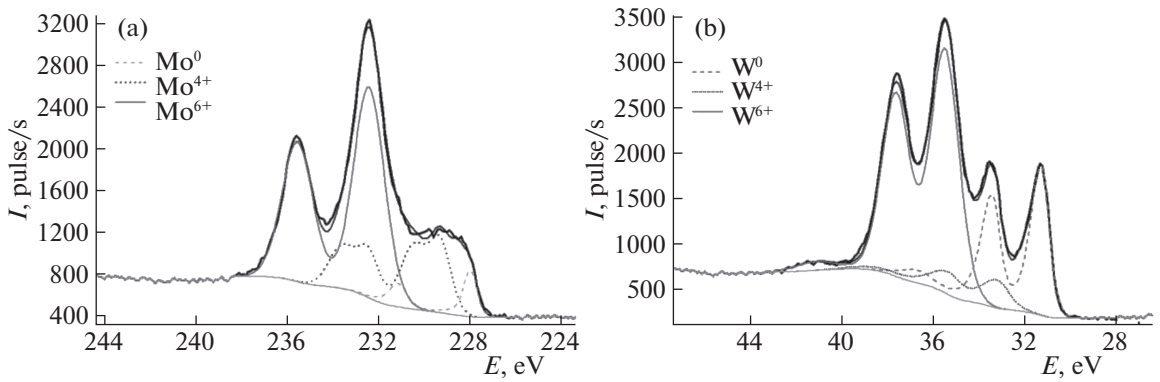

Fig. 5. Mo3*d* and W4*f* XPS spectra of samples (a) **1** and (b) **2**.

time, we cannot exclude the possibility that small amounts of other oxidized forms of molybdenum and tungsten were also present.

As can be seen from Fig. 6, the spectra of Ni2*p* and W4$f_{7/2}$ in NiW samples **3** (Figs. 6a–b) and **3-Zh** (Figs. 6c–6d) on AOK-63-11 with small granules differ from the ones shown above in Figs. 4 and 5. The proportion of lines corresponding to the Ni^0 and W^0 metallic states in them is much lower, and components attributed to the oxidized states of Ni^{+2}, W^{+4}, and W^{+6} predominate. The results from decomposing the Ni2*p* and W4$f_{7/2}$ XPS spectra into components are given in Table 4. The stronger oxidation of the metals on the surfaces of small aluminum oxide granules could be due to the larger geometric surface area of the latter, and thus to the lower surface density of the particles. A similar pattern was observed in [8] for nickel nanoparticles deposited on surfaces of alumina.

Table 3. Bonding energies (*E*) of nickel, molybdenum, and aluminum components in the XPS spectra of sample **1**, their fractions (γ), and the types of bonds corresponding to them

Spectrum	*E*, eV	γ, %	Bond type
Ni2$p_{3/2}$	852.8	19	Ni^0
	855.9	81	Ni^{+2}
Mo3$d_{5/2}$	228.0	7	Mo^0
	229.4	35	Mo^{+4}
	232.4	58	Mo^{+6}
Al 2*p*	74.8	100	Al^{+3}

Treating sample **3** with an ionic liquid (**3-IL**) greatly reduced the content of Ni and W on its surface, as was evident from the weaker intensity of the signals (Fig. 6). According to data from our XPS analysis of its surface composition, C, S, and N were present in addition to Al, Ni, W, and O, the main components of the catalyst. The carbon content was more than 60 at %, testifying to the adsorption of the ionic liquid on the surface. This is consistent with the strong drop in the specific surface area and pore volume of sample **3** after treating it with the ionic liquid. The shapes of the spectra show the Ni^0 and W^0 metallic states are missing from sample **3-IL**. These changes could be due to the oxidation of metal nanoparticles in air when

Table 4. Bonding energies of the nickel, tungsten, and aluminum components in the XPS spectra of NiW/Al_2O_3 samples (**2**, **3**, and **3-IL**), their fractions, and the types of bonds corresponding to them

Spectrum		Ni2$p_{3/2}$		W4$f_{7/2}$			Al2p
E, eV		852.5–852.7	855.9–856.2	31.1–31.3	33.2–33.6	35.4–35.8	74.7
Bond type		Ni^0	Ni^{+2}	W^0	W^{+4}	W^{+6}	Al^{+3}
γ, at % γ, wt %	**2**	28	72	28	12	60	100
	3	2	98	17	–	83	100
	3-IL	–	100	–	22	78	

the catalyst is treated with an aqueous solution of a highly polar IL [29].

Catalytic Oxidation of Thiophene Derivatives

The catalytic properties of the samples were determined in model reactions of the peroxide oxidation of thiophene and dibenzothiophene, along with desulfurization of the diesel fraction obtained at a refinery of the Khanty-Mansiysk Autonomous Okrug.

The results from testing catalysts **1**–**3** in the oxidation of thiophene are given in Table 5. As can be seen, sample **2** used in a single load produced the best results. The rate of the reaction, the TOF value, and the degree of thiophene conversion reached their maximum values in 4 h. Samples **1** and **3** (Mo- and W-containing catalysts) under these conditions demonstrated approximately the same specific atomic activity (TOF), along with similar degrees of thiophene conversion. It was therefore of interest to compare their properties under the fractional loading of H_2O_2. As can be seen from Table 5, the degree of thiophene conversion under these conditions (43 to 56%) grew notably on catalyst **1** but changed only slightly on

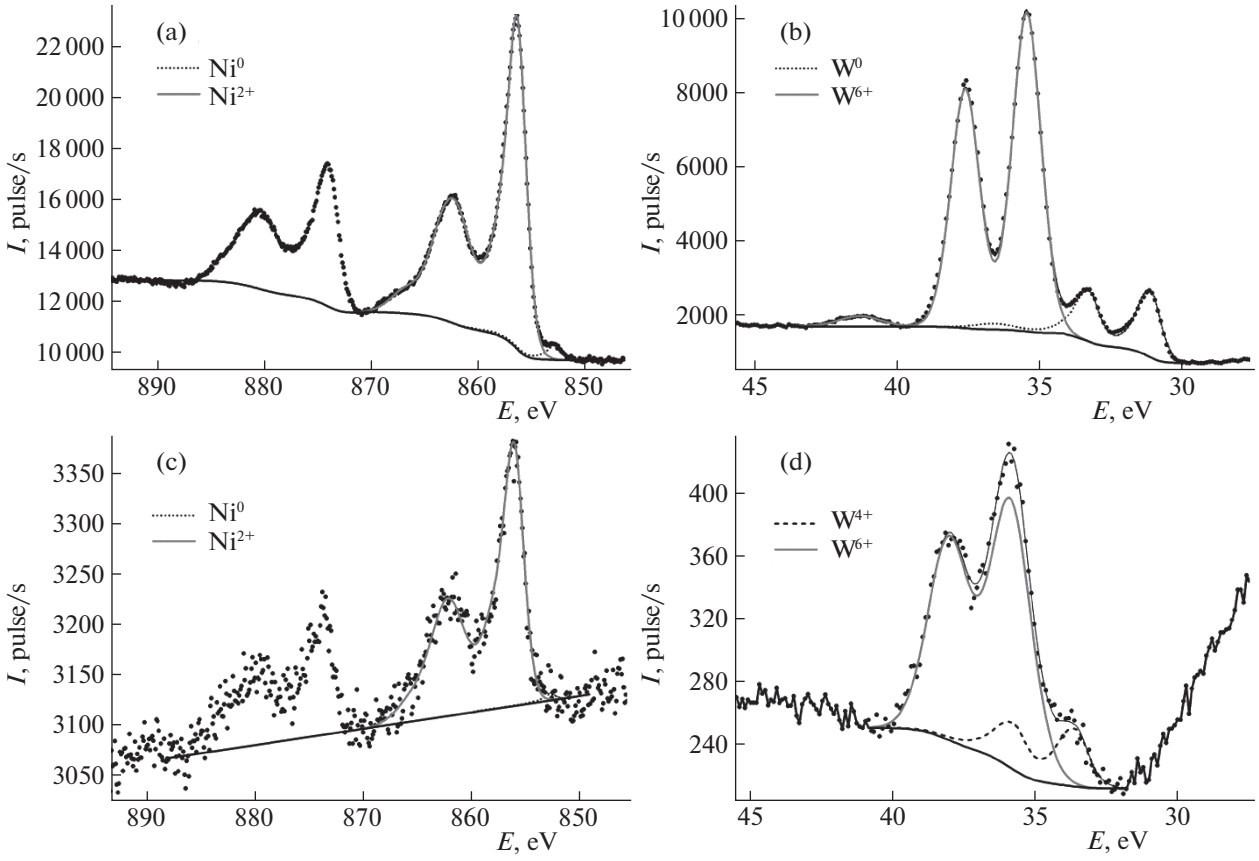

Fig. 6. Ni2p and W4f XPS spectra of samples (a–b) **3** and (c–d) **3-IL**.

Table 5. Catalytic properties of the samples in the oxidation of thiophene

Catalyst	**1**	**2**	**3**
r_o, mol/h*	0.018	0.023	0.009
TOF (1/h), Δn (thiophene)/(n (W or Mo) h)	4500	6800	5000
S_1, %	41	53	43
S_2, %	56		49

r_o is the initial rate of thiophene oxidation, S_1 is the degree of conversion of thiophene for 4 h, and S_2 is the degree of conversion of thiophene over 4 h with the fractional loading of H_2O_2 (0.2 mL + 0.2 mL with an interval of 2 h).

*60 C, 10 mL of a thiophene/*iso*-octane solution, 0.4 mL of a 50% aqueous solution of H_2O_2, and M_{cat} = 0.1 g.

catalyst **3**. This effect was apparently associated with a higher rate of H_2O_2 decomposition on Mo-containing systems, and the fractional loading of hydrogen peroxide allows us to reduce its consumption for this side reaction [24]. Analysis of the data presented in Table 5 shows this effect was weaker for W-containing catalyst **3**. The extremely high TOF value for all three catalysts, which is several orders of magnitude higher than the literature data for oxides of W and Mo [30], should also be noted. This value is somewhat conditional, as it does not include the contribution from NiO because (according to the literature [23]) its activity is much lower than that of derivatives of group VI. Nevertheless, it could be the contribution from NiO that produces the higher TOF value for catalyst **2**, since its content in this catalyst is greater than in catalyst **3**. However, we believe nickel on the surface of the carrier can in this case act as adsorption sites, while the oxidation sites are derivatives of W and Mo in high states of oxidation.

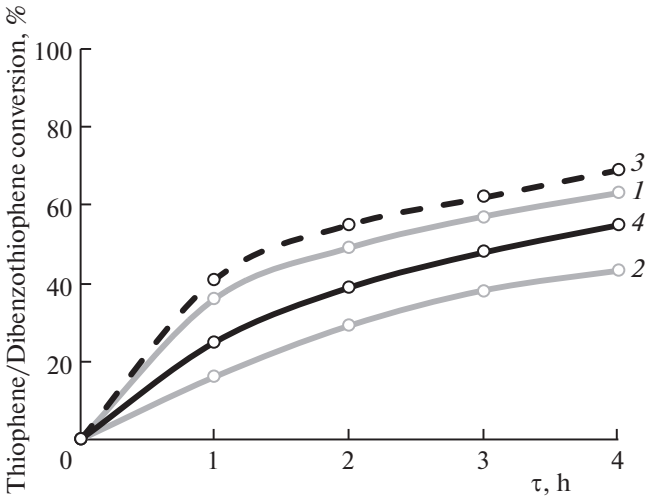

Fig. 7. Kinetic curves of substrate conversion in the presence of catalysts **3** and **3-IL** (60°C; 10 mL of a 1% solution of thiophene (DBT); 0.4 mL of a 50% aqueous solution of H_2O_2; M_{cat} = 0.1 g).

Figure 7 shows the kinetic curves of conversion for two substrates, thiophene and dibenzothiophene, in the presence of samples **3** and **3-IL**. As can be seen, introducing IL raises the degree of conversion of substrates, which is associated with its participation in adsorption [24].

However, IL also serves to stabilize the catalyst, since its surface changes substantially without it and there is a partial washout of the metallic coating. This effect is especially pronounced in thiophene oxidation, since sulfuric acid is present among the conversion products. This can be seen by comparing microphotographs of the surfaces of samples **3** and **3-IL** after their use in the oxidation of thiophene (Fig. 8).

Figure 9 presents data on the stability of catalyst **3-IL** in five consecutive cycles of the peroxide oxidation of thiophene and dibenzothiophene.

Analysis of Figs. 7–9 shows that adding a zwitterionic liquid raises the degree of conversion further and improves the resistance of the catalyst's surface to the action of the reaction medium, including the sulfuric acid produced during the oxidation of substrates.

The effect of IL was weaker in the oxidation of sulfur in diesel fuel: the total degree of conversion of S when using a single load of H_2O_2 was 82% on catalyst **3** (residual S content, 199 ppm) and 84% on catalyst **3-IL** (169 ppm). It proved more effective to use the fractional loading of H_2O_2. As a result, the degree of S conversion exceeded 90%, and the residual content of S after processing the diesel fuel was 92 ppm on catalyst **3** and 88 ppm on catalyst **3-IL**.

CONCLUSIONS

Laser electrodispersion of targets made from pressed mixtures of Ni and Mo or W powders allowed us to obtain bimetallic nanostructured coatings with given ratios of mixture components and their uniform distribution over the surfaces of aluminum oxide granules. The coating components were present on the surfaces of samples in the metallic and oxidized states, in the form of nanoparticles of 4–7 nm in size. The degree of oxidation and the proportion of the oxidized states of the metals were determined from the surface density of the particles. These samples with extremely low contents of active ingredients of less than 7×10^{-3} wt % were active in the oxidation of thiophene and dibenzothiophene by hydrogen peroxide. The degrees of conversion of the initial substrates on them were comparable to or even exceeded the values obtained on known catalysts with substantially higher metal contents. High values of conversion were retained when the catalysts were used repeatedly. Adding a zwitterionic liquid to the reaction mixture contributed to an addi-

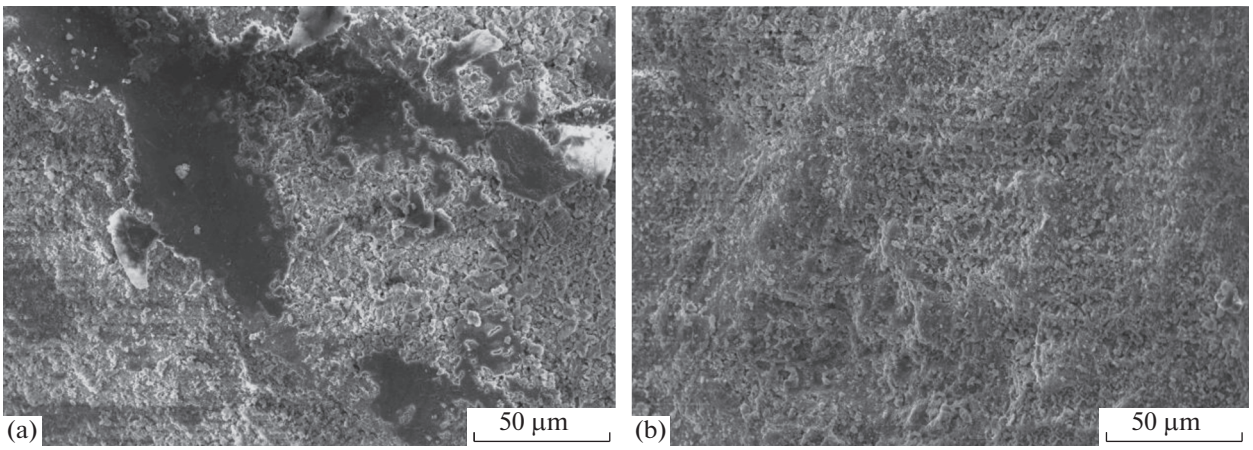

Fig. 8. SEM images of samples **3** and **3-IL** after five cycles of the catalytic reaction.

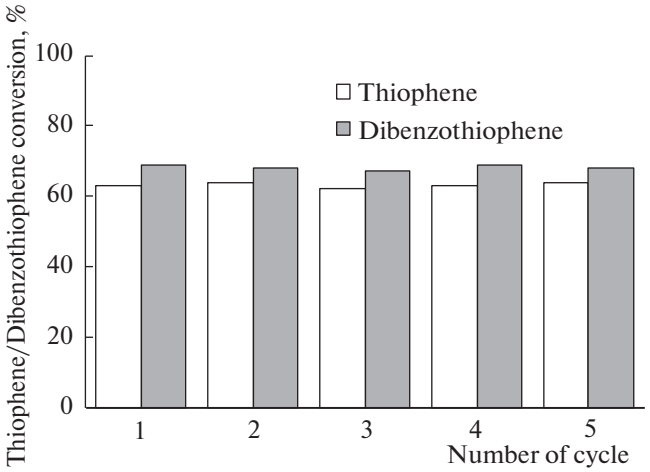

Fig. 9. Conversion of substrates in the presence of catalyst **3-IL** over five consecutive cycles (60°C; 10 mL of a 1% solution of thiophene (DBT); 0.4 mL of a 50% aqueous solution of H_2O_2; M_{cat} = 0.1 g).

tional increase in the degree of conversion and the resistance of the catalyst's surface to the action of the reaction medium, including the sulfuric acid produced during the oxidation of substrates. The prospects for using highly active and stable catalysts in the oxidative desulfurization of diesel fuels were shown.

FUNDING

This work was performed using equipment purchased under the Program for the Competitive Growth of Moscow State University. The catalyst structures were formed as part of a State Task for the Ioffe Institute of Physics and Technology, Russian Academy of Sciences.

REFERENCES

1. S. Hong, H. Lee, J. Yeo, and S. Hwan Ko, Nano Today **11**, 547 (2016).
2. J. Zhang, M. Chaker, and D. Ma, J. Colloid Interface Sci. **489**, 138 (2017).
3. V. S. Rudnev, I. V. Lukiyanchuk, M. S. Vasilyeva, et al., Appl. Surf. Sci. **422**, 1007 (2017).
4. E. S. Lokteva, A. A. Peristyy, N. E. Kavalerskaya, et al., Pure Appl. Chem. **84**, 495 (2012).
5. E. V. Golubina, T. N. Rostovshchikova, E. S. Lokteva, et al., Pure Appl. Chem. **90**, 1685 (2018).
6. T. N. Rostovshchikova, E. S. Lokteva, E. V. Golubina, K. I. Maslakov, S. A. Gurevich, D. A. Yavsin, and V. M. Kozhevin, in *Advanced Nanomaterials for Catalysis and Energy: Synthesis, Characterization and Application,* Ed. by V. Sadykov (Elsevier, Amsterdam, 2019), p. 61.
7. E. V. Golubina, E. S. Lokteva, K. I. Maslakov, T. N. Rostovshchikova, M. I. Shilina, S. A. Gurevich, V. M. Kozhevin, and D. A. Yavsin, Nanotechnol. Russ. **12**, 19 (2017).
8. N. E. Kavalerskaya, E. S. Lokteva, T. N. Rostovshchikova, E. V. Golubina, and K. I. Maslakov, Kinet. Catal. **54**, 597 (2013).
9. T. N. Rostovshchikova, M. I. Shilina, E. V. Golubina, E. S. Lokteva, I. N. Krotova, S. A. Nikolaev, K. I. Maslakov, and D. A. Yavsin, Russ. Chem. Bull. **64**, 812 (2015).
10. A. K. Gatin, M. V. Grishin, S. A. Gurevich, N. V. Dokhlikova, A. A. Kirsankin, V. M. Kozhevin, E. S. Lokteva, T. N. Rostovshchikova, S. Yu. Sarvadii, B. R. Shub, and D. A. Yavsin, Russ. Chem. Bull. **64**, 2337 (2015).
11. F. S. Mjalli, O. U. Ahmed, T. Al-Wahaibi, et al., Rev. Chem. Eng. **30**, 337 (2014).
12. V. C. Srivastava, RSC Adv. **2**, 759 (2012).
13. Y. N. Prajapati and N. Verma, Fuel **216**, 381 (2018).
14. W. N. W. Abdullah, W. A. W. Abu Bakar, R. Ali, et al., J. Clean. Prod. **162**, 1455 (2017).
15. E. V. Rakhmanov, A. V. Tarakanova, A. V. Akopyan, et al., Pet. Chem. **54**, 48 (2014).

16. L. C. A. de Oliveira, N. T. Costa, J. R. Pliego, et al., Appl. Catal., B **147**, 43 (2014).
17. Y. Muhammad, A. Shoukat, A. U. Rahman, et al., Chin. J. Chem. Eng. **26**, 593 (2018).
18. A. Waqas, *Sulfur in Petroleum: Petroleum Desulfurization Techniques Applying Nanotechnology to the Desulfurization Process in Petroleum Engineering* (IGI Global, Hershey, PA, 2016), p. 1.
19. Z. Hasan, J. Jeon, and S. H. Jhung, J. Hazard. Mater. **205–206,** 216 (2012).
20. P. Polikarpova, A. Akopyan, A. Shigapova, et al., Energy Fuels **32**, 10898 (2018).
21. W. Abdul-Kadhim, M. A. Deraman, S. B. Abdullah, et al., J. Environ. Chem. Eng. **5**, 1645 (2017).
22. Wan Nazwanie Wan Abdullah, Wan Azelee Wan Abu Bakar, Rusmidah Ali, et al., J. Clean. Prod. **162**, 1455 (2017).
23. Z. Ismagilov, S. Yashnik, M. Kerzhentsev, et al., Catal. Rev. Sci. Eng. **53**, 199 (2011).
24. I. G. Tarkhanova, A. A. Bryzhin, M. G. Gantman, et al., Surf. Coat. Technol. **362**, 132 (2019).
25. Q. Wu, W. J. Li, M. Wang, et al., RSC Adv. **5**, 57968 (2015).
26. J. F. Moulder, W. F. Stickle, P. E. Sobol, and K. D. Bomben, *Handbook of X-ray Photoelectron Spectroscopy* (ULVAC-PHI, Chigasaki, 1995).
27. A. N. Mansour, Surf. Sci. Spectra **3**, 231 (1994).
28. D. O. Scanlon, G. W. Watson, D. J. Payne, et al., J. Phys. Chem. C **114**, 4636 (2010).
29. H. Ohno, M. Yoshizawa-Fujita, Y. Kohno, et al., Phys. Chem. Chem. Phys. **20**, 10978 (2018).
30. B. Zhang, Z. Jiang, J. Li, et al., J. Catal. **287**, 5 (2012).

Translated by O. Kadkin

SPELL: OK